Ann. Geophys. Discuss., https://doi.org/10.5194/angeo-2018-63
Manuscript under review for journal Ann. Geophys.
Discussion started: 3 July 2018

Annales Geophysicae Discussions
Open Access
EGU

Local time extent of magnetopause reconnection X-lines using space-ground coordination

Ying Zou[1,2], Brian M. Walsh[3], Yukitoshi Nishimura[4,5], Vassilis Angelopoulos[6], J. Michael Ruohoniemi[7], Kathryn A. McWilliams[8], Nozomu Nishitani[9]

1. Department of Astronomy and Center for Space Physics, Boston University, Massachusetts, USA
2. Cooperative Programs for the Advancement of Earth System Science, University Corporation for Atmospheric Research, Boulder, Colorado, USA
3. Department of Mechanical Engineering and Center for Space Physics, Boston University, Boston, Massachusetts, USA
4. Department of Electrical and Computer Engineering and Center for Space Sciences, Boston University, Boston, Massachusetts, USA
5. Department of Atmospheric and Oceanic Sciences, University of California, Los Angeles, California, USA
6. Department of Earth, Planetary and Space Sciences, University of California, Los Angeles, California, USA
7. The Bradley Department of Electrical and Computer Engineering, Virginia Tech, Blacksburg, Virginia, USA
8. Institute of Space and Atmospheric Studies, University of Saskatchewan, Saskatoon, Saskatchewan, Canada
9. Center for International Collaborative Research, Institute for Space-Earth Environmental Research, Nagoya University, Nagoya, Japan

Ann. Geophys. Discuss., https://doi.org/10.5194/angeo-2018-63
Manuscript under review for journal Ann. Geophys.
Discussion started: 3 July 2018

Corresponding author: Ying Zou

1. Department of Astronomy and Center for Space Physics, Boston University, Massachusetts, USA

2. Cooperative Programs for the Advancement of Earth System Science, University Corporation for Atmospheric Research, Boulder, Colorado, USA

yingzou@bu.edu

Keyword: 2784 Solar wind–magnetosphere interactions; 2724 Magnetopause, cusp, and boundary layers; 7835 Magnetic reconnection

Ann. Geophys. Discuss., https://doi.org/10.5194/angeo-2018-63
Manuscript under review for journal Ann. Geophys.
Discussion started: 3 July 2018

Annales Geophysicae Discussions
Open Access
EGU

47 Abstract

48 Magnetic reconnection X-lines can vary considerably in length. At the Earth's magnetopause,
49 the length generally corresponds to the extent in local time. The extent has been probed by multi-
50 spacecraft crossing the magnetopause, but the estimates have large uncertainties because of the
51 assumption of a continuous X-line between spacecraft and the lack of information beyond areas of
52 spacecraft coverage. The extent has also been inferred by radars as fast ionospheric flows moving
53 anti-sunward across the open-closed field line boundary, but whether a particular ionospheric flow
54 results from reconnection needs to be confirmed. To achieve a reliable interpretation, we compare
55 X-line extents probed by multi-spacecraft and radars for three conjunction events. We find that
56 when reconnection is active at only one spacecraft, only the ionosphere conjugate to this spacecraft
57 shows a channel of fast anti-sunward flow. When reconnection is active at two spacecraft and the
58 spacecraft are separated by <1 Re, the ionosphere conjugate to both spacecraft shows a channel of
59 fast anti-sunward flow. The consistency allows us to determine the X-line extent by measuring the
60 ionospheric flows. The flow extent is 520, 572, and 1260 km, corresponding to an X-line extent
61 of 4, 5, and 11 Re. This strongly indicates that both spatially patchy (a few Re) and spatially
62 continuous and extended reconnection (>10 Re) are possible forms of reconnection at the
63 magnetopause. Interestingly, the extended reconnection develops from a localized patch via
64 spreading across local time. Potential effects of IMF Bx and By on the X-line extent are discussed.

65

66

67

68

69

Ann. Geophys. Discuss., https://doi.org/10.5194/angeo-2018-63
Manuscript under review for journal Ann. Geophys.
Discussion started: 3 July 2018

1. Introduction

A long-standing question in magnetic reconnection is what is the spatial extent of reconnection in the direction normal to the reconnection plane. At the Earth's magnetopause, for a purely southward IMF, this corresponds to the extent in the local time or azimuthal direction. The extent of reconnection has significant relevance to solar wind-magnetosphere coupling, as it controls the amount of energy being passed through the boundary from the solar wind into the magnetosphere and ionosphere. Magnetopause reconnection tends to occur at sites of strictly anti-parallel magnetic fields as anti-parallel reconnection [e.g. *Crooker*, 1979; *Luhmann et al.*, 1984], or occur along a line passing through the subsolar region as component reconnection [e.g. *Sonnerup*, 1974; *Gonzalez and Mozer*, 1974]. This, however, does not represent the extent of active reconnection X-lines, as reconnection may not be active at all portions of this configuration, but can occur at discontinuous patches or over a limited segment only.

Numerical models show that reconnection tends to occur at magnetic separators, i.e. at the junction between regions of different magnetic field topologies, and global MHD models have identified a spatially continuous separator along the magnetopause [*Dorelli et al.*, 2007; *Laitinen et al.*, 2006, 2007; *Haynes and Parnell*, 2010; *Komar et al.*, 2013; *Glocer et al.*, 2016]. However, little is known about where and over what range along the separators reconnection is active. Reconnection in numerical simulations can be activated by introducing perturbations of the magnetic field or can grow spontaneously with instability or resistivity inherent in the system [e.g. *Hesse et al.*, 2001; *Scholer et al.*, 2003]. When reconnection develops as patches (as due to the instabilities or localized perturbations), the patches can spread in the direction out of the reconnection plane [*Huba and Rudakov*, 2002; *Shay et al.* 2003; *Lapenta et al.*, 2006; *Nakamura et al.*, 2012; *Shepherd and Cassak*, 2012; *Jain et al.*, 2013]. The patches either remain patchy after

Ann. Geophys. Discuss., https://doi.org/10.5194/angeo-2018-63
Manuscript under review for journal Ann. Geophys.
Discussion started: 3 July 2018

93 spreading if the current layer is thick, or form an extended X-line if the current layer is already
94 thin [*Shay et al.*, 2003].

95 The extent of reconnection X-lines has been observationally determined based on fortuitous
96 satellite conjunctions where the satellites detect signatures of active reconnection at the
97 magnetopause at different local times nearly simultaneously [*Phan et al.*, 2000, 2006; *Walsh et*
98 *al.*, 2014a, 2014b, 2017]. The satellites were separated by a few Re in *Phan et al.* [2000] and *Walsh*
99 *et al.* [2014a, 2014b, 2017], and >10 Re in *Phan et al.* [2006], and this is interpreted as the X-line
100 being longer than a few Re and even 10 Re, respectively. At the magnetopause, X-lines of a few
101 Re are often referred to as spatially patchy [e.g., *Fear et al.*, 2008, 2010], and X-lines of >10 Re
102 are spatially extended [*Dunlop et al.*, 2011; *Hasegawa et al.*, 2016]. The extent of X-lines has been
103 alternatively determined by studying the structures of newly reconnected flux tubes, i.e., flux
104 transfer events (FTEs) [*Russell and Elphic*, 1978; *Haerendel et al.*, 1978]. Conceptual models
105 regard FTEs either as azimuthally narrow flux tubes that intersect the magnetopause through nearly
106 circular holes, as formed by spatially patchy X-lines [*Russell and Elphic*, 1978], or as azimuthally
107 elongated bulge structures or flux ropes that extend along the magnetopause, as formed by spatially
108 extended X-lines [*Scholer*, 1988; *Southwood et al.*, 1987; *Lee and Fu*, 1985]. FTEs have been
109 observed to be > or <2 Re wide in local time [*Fear et al.*, 2008, 2010; *Wang et al.*, 2005, 2007].
110 FTEs have even been observed across ~20 Re from the subsolar region to the flanks [*Dunlop et*
111 *al.*, 2011]. But it is unclear whether these FTEs are branches of one extended bulge or flux rope,
112 or multiple narrow tubes formed simultaneously. When the satellites are widely spaced, it is in
113 general questionable whether an X-line/FTE is spatially continuous between the satellites or
114 whether satellites detect the same moving X-line/FTE. Satellites with a small separation may
115 possibly measure the same X-line/FTE, but only provide a lower limit estimate of the extent. An

Ann. Geophys. Discuss., https://doi.org/10.5194/angeo-2018-63
Manuscript under review for journal Ann. Geophys.
Discussion started: 3 July 2018

116 X-line/FTE may also propagate or spread between satellite detection but satellite measurements
117 cannot differentiate the spatial and temporal effects.

118 This situation can be improved by studying ionospheric signatures of reconnection and FTEs,
119 since their spatial sizes in the ionosphere can be obtained from wide field ground instruments or
120 Low-Earth orbit spacecraft. The ionospheric signatures include poleward moving auroral forms
121 (PMAFs), channels of fast flows moving anti-sunward across the open-closed field line boundary
122 [e.g., *Southwood*, 1985], and cusp precipitation [*Lockwood and Smith*, 1989, 1994; *Smith et al.*,
123 1992]. Radar studies have shown that the flows can differ considerably in size, varying from tens of
124 km [*Oksavik et al.*, 2004, 2005], to hundreds of km [*Goertz et al.*, 1985; *Pinnock et al.*, 1993, 1995;
125 *Provan and Yeoman*, 1999; *Thorolfsson et al.*, 2000; *McWilliams et al.*, 2001a, 2001b], and to
126 thousands of km [*Provan et al.*, 1998; *Nishitani et al.*, 1999; *Provan and Yeoman*, 1999]. A
127 similarly broad distribution has been found for PMAFs [e.g. *Sandholt et al.*, 1986, 1990; *Lockwood*
128 *et al.*, 1989, 1990; *Milan et al.*, 2000, 2016] and the cusp [*Crooker et al.*, 1991; *Newell and Meng*,
129 1994; *Newell et al.*, 2007]. This range of spatial sizes in the ionosphere approximately corresponds
130 to a range from <1 to >10 Re at the magnetopause. However, care needs to be taken when
131 interpreting the above ionospheric features, since they could also form due to other drivings such
132 as solar wind dynamic pressure pulses [*Lui and Sibeck*, 1991; *Sandholt et al.*, 1994]. An
133 unambiguous proof of their connection to magnetopause reconnection requires simultaneous
134 space-ground coordination [*Elphic et al.*, 1990; *Denig et al.*, 1993; *Neudegg et al.*, 1999, 2000;
135 *Lockwood et al.*. 2001; *Wild et al.*, 2001, 2005, 2007; *McWilliams et al.*, 2004; *Zhang et al.*, 2008].

136 Therefore a reliable interpretation of reconnection X-line extent has been difficult due to
137 observation limitations. We will address this by comparing X-line extents probed by multi-
138 spacecraft and radars using space-ground coordination. On one hand, this enables us to investigate

Ann. Geophys. Discuss., https://doi.org/10.5194/angeo-2018-63
Manuscript under review for journal Ann. Geophys.
Discussion started: 3 July 2018

whether X-lines are continuous between satellites, and how wide X-lines extends beyond satellites. On the other hand, this helps to determine whether reconnection is the driver of ionospheric disturbances and whether the in-situ extent is consistent with the ionospheric disturbance extent.

It may be noteworthy to point out that we only address the X-line extent in the local time direction, similarly to previous observations. If the X-line has a tilted orientation relative to the equatorial plane, the local time extent will be shorter than the total extent. How X-lines tilt is a subject of ongoing research. Various models have been proposed to predict the tilt [*Alexeev et al.*, 1998; *Moore et al.*, 2002; *Trattner et al.*, 2007; *Swisdak and Drake*, 2007; *Borovsky*, 2013; *Hesse et al.*, 2013] but their performance is still under test [e.g., *Komar et al.*, 2015]. The local time extent is what determines the amount of magnetic flux opened in the solar wind-magnetopshere coupling [e.g. *Newell et al.*, 2007].

2. Methodology

We use conjugate measurements between the Time History of Events and Macroscale Interactions during Substorms (THEMIS) [*Angelopoulos*, 2008] and Super Dual Auroral Network (SuperDARN) [*Greenwald et al.*, 1995]. We focus on intervals when the IMF in OMNI data remains steadily southward. We require that two of the THEMIS satellites fully cross the magnetopause nearly simultaneously and that the satellite data provide clear evidence for reconnection occurring or not. The full crossings are identified by a reversal of the Bz magnetic field and a change in the ion energy spectra. The requirements of nearly simultaneous crossings and steady IMF conditions help to reduce the spatial-temporal ambiguity by satellite measurements, where the presence/absence of reconnection signatures at different local times likely reflects spatial structures of reconnection. Reconnection can still possibly vary between the two satellite crossings, and we use the radar measurements to examine whether the reconnection X-line of

Ann. Geophys. Discuss., https://doi.org/10.5194/angeo-2018-63
Manuscript under review for journal Ann. Geophys.
Discussion started: 3 July 2018

interest has continued to exist and maintained its spatial size.

Fluid (MHD) evidence of magnetopause reconnection includes plasma bulk flow acceleration at the magnetopause. This acceleration should be consistent with the prediction of tangential stress balance across a rotational discontinuity, i.e. Walen relation [*Hudson*, 1970; *Paschmann et al.*, 1979]. The Walen relation is expressed as

$$\Delta V_{predicted} = \pm(1-\alpha_1)^{1/2}(\mu_o\rho_1)^{-1/2}[B_2(1-\alpha_2)/(1-\alpha_1) - B_1] \qquad (1)$$

Where ΔV is the change in the plasma bulk velocity vector across the discontinuity. B and ρ are the magnetic field vector and plasma mass density. μ_0 is the vacuum permeability. $\alpha = (p_{\parallel} - p_{\perp})\mu_0/B^2$ is the anisotropy factor where $p_{\parallel}$ and $p_{\perp}$ are the plasma pressures parallel and perpendicular to the magnetic field. The magnetic field and plasma moments are obtained from the fluxgate magnetometer (FGM) [*Auster et al.*, 2008] and the ElectroStatic Analyzers (ESA) instrument [*McFadden et al.*, 2008]. The plasma mass density is determined using the ion number density, assuming a mixture of 95% protons and 5% helium. The subscripts 1 and 2 refer to the reference interval in the magnetosheath and to a point within the magnetopause, respectively. The magnetosheath reference interval is a 10-s time period just outside the magnetopause. The point within the magnetopause is taken at the maximum ion velocity change across the magnetopause. We ensure that the plasma density at this point is >20% of the magnetosheath density to avoid the slow-mode expansion fan [*Phan et al.*, 1996]. We compare the observed ion velocity change with the prediction from the Walen relation. The level of agreement is measured by $\Delta V^* = \Delta V_{obs} \cdot \Delta V_{predicted} \Big/ |\Delta V_{predicted}|^2$, following *Paschmann et al.* [1986]. Here $\Delta Vobs$ is the observed ion velocity change.

A kinetic signature of reconnection is found as D-shaped ion distributions at the magnetopause. As magnetosheath ions encounter newly opened magnetic field lines at the magnetopause, they

Ann. Geophys. Discuss., https://doi.org/10.5194/angeo-2018-63
Manuscript under review for journal Ann. Geophys.
Discussion started: 3 July 2018

either transmit through the magnetopause entering the magnetosphere or reflect at the boundary. The transmitted ions have a cutoff parallel velocity (i.e. de-Hoffman Teller velocity) below which no ions could enter the magnetosphere. The D-shaped ion distributions persist from the active reconnection region at the magnetopause into the ionosphere where they appear as cusp ion steps [*McWilliams et al.*, 2004]. We require the satellites to operate in the Fast Survey or Burst mode in which ion distributions are available at 3 s resolution.

We determine reconnection being active if the plasma velocity change across the magnetopause is consistent with the Walen relation with $\Delta V^{*} >= 0.5$, and if the ions at the magnetopause show a D shape distribution. Reconnection is deemed absent if neither of the two signatures is detected. We require that at least one of the two satellites observe reconnection signatures. Reconnection is regarded as ambiguous if only one of the two signatures is detected, and such reconnection is excluded from our analysis.

We mainly use the three SuperDARN radars located at Rankin Inlet (RKN, geomagnetic 72.6° MLAT, -26.4° MLON), Inuvik (INV, 71.5° MLAT, -85.1° MLON), and Clyde River (CLY, 78.8° MLAT, 18.1° MLON) to measure the ionospheric convection near the dayside cusp. The three radars have overlapping field of views (FOVs), enabling a reliable determination of the 2-d convection velocity. The FOVs cover the ionosphere >75° MLAT, covering the typical location of the cusp under weak and modest solar wind driving conditions [i.e., *Newell et al.*, 1989] and the high occurrence region of pulsed ionospheric flows [*Provan and Yeoman*, 1999] with high spatial resolution. Data from Saskatoon (SAS, 60° MLAT, -43.8° MLON) and Prince George (PGR, 59.6° MLAT, -64.3° MLON) radars are also used when data are available. The measurements of these two radars at far range gates can overlap with the cusp. The radar data have a time resolution of 1-2 min. We focus on observations ±3 h MLT from magnetic noon (approximately 1600-2200 UT).

Ann. Geophys. Discuss., https://doi.org/10.5194/angeo-2018-63
Manuscript under review for journal Ann. Geophys.
Discussion started: 3 July 2018

209 The satellite footprints should be mapped close to the radar FOVs under the Tsyganenko (T89)
210 model [*Tsyganenko*, 1989]. Footprints mapped using different Tsyganenko (e.g., T96 or T01
211 [*Tsyganenko*, 1995, 2002a, 2002b]) models have similar longitudinal locations (difference <100
212 km), implying the longitudinal uncertainty of mapping to be small. The latitudinal uncertainty can
213 be inferred by referring to the open-closed field line boundary as estimated using the 150 m/s
214 spectral width boundary [e.g., *Baker et al.*, 1995, 1997; *Chisham and Freeman*, 2003]. And T89
215 has given the smallest latitudinal uncertainty for the studied events. We surveyed years 2014-2016
216 during the months when the satellite apogee was on the dayside, and found 6 such conjunctions.
217 The ionospheric signature of reconnection includes fast anti-sunward flows moving across the
218 open-closed field line boundary. We obtain the flow velocity vectors by merging line-of-sight
219 (LOS) measurements at the radar common FOVs [*Ruohoniemi and Baker*, 1998], and these merged
220 vectors reflect the true ionospheric convection velocity. However, the radar common FOVs are
221 hundreds of km wide only, which can be too small to cover the full azimuthal extent of the
222 reconnection-related flows (which are up to thousands of km wide). We therefore also reconstruct
223 the velocity field using the Spherical Elementary Current Systems (SECS) method [*Amm et al.*,
224 2010]. Similar to the works by *Ruohoniemi et al.* [1989] and *Bristow et al.* [2016], the SECS
225 method reconstructs a divergence-free flow pattern using all LOS velocity data. We refer to these
226 velocities as SECS velocities. The accuracy of SECS velocities can be validated by comparing to
227 the LOS measurements and the merged vectors. SECS velocities work best in regions with dense
228 echo coverage and those around sparse echoes are not reliable and thus are excluded from our
229 analysis.
230 The third way of obtaining a velocity field is Spherical Harmonic Fit (SHF). This method uses
231 the LOS measurements and a statistical convection model to fit the distribution of electrostatic

Ann. Geophys. Discuss., https://doi.org/10.5194/angeo-2018-63
Manuscript under review for journal Ann. Geophys.
Discussion started: 3 July 2018

potential, which is expressed as a sum of spherical harmonic functions [*Ruohoniemi and Baker*, 1998]. The statistical model employed here is *Cousins and Shepherd* [2010]. While this method may suppress small or meso-scale velocity details, such as, sharp flow gradients or flow vortices, we compare SHF velocities with the LOS measurements and merged vectors to determine how well the SHF velocities depict the velocity details.

Among the six events we identified, we present three representative conjunction events in Sections 3.1-3.3. The time separation of magnetopause crossings by two satellites are 1, 2, and 30 min. While the time separation for the third case is somewhat long, we distinguish the spatial and temporal effects using the radar data. Although the three events occurred under similar IMF Bz conditions, the reconnection-related flows in the ionosphere had an azimuthal extent varying from a few hundred km (Sections 3.1-3.2) to more than a thousand km wide (Section 3.3). This corresponds to X-lines of a few to >10 Re long, indicating that both spatially patchy (a few Re) and spatially continuous and extended reconnection (>10 Re) are possible forms of reconnection at the magnetopause. Interestingly, extended reconnection was found to arise from a spatially localized patch that spreads azimuthally. Potential effects of IMF Bx and By on the reconnection extent are discussed in Section 3.4.

3. Observations

3.1. Spatially patchy reconnection active at one satellite only

3.1.1. In-situ satellite measurements

On March 11, 2014, THA and THD made simultaneous measurements of the dayside magnetopause with a 4.2 Re separation in the Y direction. The IMF condition is displayed in Figure 1a and the IMF was directed southward. The satellite location in the GSM coordinates is displayed

Ann. Geophys. Discuss., https://doi.org/10.5194/angeo-2018-63
Manuscript under review for journal Ann. Geophys.
Discussion started: 3 July 2018

255 in Figure 1b, and the measurements are presented in Figures 1c-ll. The magnetic field and the ion
256 velocity components are displayed in the LMN boundary normal coordinate system, where *L* is
257 along the outflow direction, *M* is along the X-line, and *N* is the current sheet normal. The
258 coordinate system is obtained from the minimum variance analysis of the magnetic field at each
259 magnetopause crossing [*Sonnerup and Cahill*, 1967]. Both satellites passed from the
260 magnetosphere into the magnetosheath, as seen as the sharp changes in the magnetic field, the ion
261 spectra, and the density (shaded in pink).

262 As THD crossed the magnetopause boundary layer (1624:47-1625:09 UT), it detected both fluid
263 and kinetic signatures of reconnection. It observed a rapid, northward-directed plasma jet within
264 the region where the magnetic field rotated (Figures 1c and 1f). The magnitude of this jet reached
265 138 km/s at its peak, which was 60% of the predicted speed of a reconnection jet by the Walen
266 relation (231 km/s, not shown). The angle between the observed and predicted jets was 22°. The
267 jet velocity was somewhat small (although still sufficiently large that $\Delta V^* > 0.5$) because of the
268 presence of cold magnetospheric ions seen in Figure 1g [*Phan et al.*, 2013]. Figure 1g suggests
269 that the magnetosheath ion population had a parallel velocity of ~200 km/s, and the cold
270 magnetospheric ion population had a parallel velocity near zero. Therefore although the bulk
271 velocity computed by combining the two populations was considerably slower than the Walen
272 prediction, the velocity of the magnetosheath population was actually very close to the prediction.
273 The ion distributions in Figure 1g showed a characteristic D-shaped distribution, consistent with
274 active reconnection.

275 THA crossed the magnetopause one minute earlier than THD (1623:29-1624:07 UT). While it
276 still identified a plasma jet at the magnetopause (Figures 1h and 1k), the jet speed was significantly
277 smaller than what was predicted for a reconnection jet (97 km/s versus 200 km/s). The observed

Ann. Geophys. Discuss., https://doi.org/10.5194/angeo-2018-63
Manuscript under review for journal Ann. Geophys.
Discussion started: 3 July 2018

jet was directed 21° away from the prediction. No clear D-shaped distributions have been found in the ion distributions at the magnetopause (Figure 1l). Reconnection was thus much less active at THA local time than at THD. This suggests that the X-line of the active reconnection at THD likely did not extend to THA.

3.1.2 Ground radar measurements

The velocity field of the dayside cusp ionosphere during the satellite measurements is shown in Figure 2 (the 1-min difference from the satellite magnetopause crossing time is negligible as it was within the 1-2-min radar resolution). Figure 2a shows the radar LOS measurements, as denoted by the color tiles, and the merged vectors, as denoted by the arrows. The colors of the arrows indicate the merged velocity magnitudes, and the colors of the tiles indicate the LOS speeds that direct anti-sunward (those project to the sunward direction appear as black). Fast (red) and anti-sunward flows are the feature of our interest. One channel of such flow can be identified in the pre-noon sector, which had a speed of ~700 m/s and was directed poleward and westward. The velocity vectors >~80° MLAT were directed roughly parallel to the RKN radar beams, and therefore the RKN LOS measurements represent the primary component of the flow. The flow crossed the open-closed field line boundary, which stayed quasi-steadily at 77° MLAT based on the spectral width (Figure 2d discussed below). This flow thus meets the criteria of being an ionospheric signature of magnetopause reconnection.

The flow had a limited azimuthal extent. The extent is determined at half of the maximum flow speed, which was ~400 m/s. Figure 2e discussed below shows a more quantitative estimate of the extent. In Figure 2a, we mark the eastern boundary with the dashed magenta line, across which the velocity vectors at 79°-83° MLAT dropped from red/orange to green color. Those green vectors,

Ann. Geophys. Discuss., https://doi.org/10.5194/angeo-2018-63
Manuscript under review for journal Ann. Geophys.
Discussion started: 3 July 2018

different from the red vectors, were directed mainly westward roughly in parallel to the CLY radar beams. They had a small poleward velocity component, or even an equatorward component, up to 2 h in MLT past magnetic noon as seen from the dark blue and the black LOS measurements from RKN and SAS. They hence were the slow background convection outside the fast anti-sunward flow. The western boundary of the flow had extended beyond the RKN FOV. But it did not extend more than 1.5 h in MLT beyond because the INV echoes there showed weakly poleward and equatorward LOS speeds across the open-closed field line boundary.

It is possible to infer the location of the flow western boundary more definitively from the SECS velocities than the LOS measurements. Figure 2b shows the SECS velocities, denoted by the arrows. The SECS velocities reasonably reproduced the spatial structure of the flow channel seen in Figure 2a. The flow western boundary was marked by the dashed magenta line, across which the flow speed dropped and the flow direction reversed. The equatorward-directed flows are interpreted as the return flow of the poleward flows, as sketched in *Southwood* [1987] and *Oksavik et al.* [2004].

The velocity field reconstructed using the SHF velocities is shown in Figure 2c (obtained through the Radar Software Toolkit (http://superdarn.thayer.dartmouth.edu/software.html)). The SHF velocities also exhibit a channel of fast poleward and westward directed flow, which was similar to the flow channel in Figure 2b. The flow western and eastern boundaries were again marked by the dashed magenta lines (using the same ~400-m/s threshold as above), across which the SHF velocities dropped from orange to green/blue.

We can test the reliability of the identified flow extent by referring to the extent of the cusp. Evidence has shown that the longitudinal extent of the cusp correlates with the extent of PMAFs [*Moen et al.*, 2000] and of poleward flows across the open-closed field line boundary [*Pinnock*

Ann. Geophys. Discuss., https://doi.org/10.5194/angeo-2018-63
Manuscript under review for journal Ann. Geophys.
Discussion started: 3 July 2018

and Rodger, 2001]. Figure 2d shows spectral width measurements and the cusp can be identified as a region of high spectral widths (red color) as circled in the red contour. The cusp was located at the western half of the RKN FOV and its eastern edge corresponded to a drop of the spectral widths from red to green color. The western edge extended beyond the RKN FOV and the extension was partially captured by the PGR echoes (marked by the dashed line as the backscatters there had gaps in space and were sporadic in time). But it ended around the low spectral widths of the CLY backscatters eastward of the INV FOV. The location and the extent of the cusp therefore support the location and the extent of the anti-sunward flow.

The limited extent of the flow did not vary much in time, as suggested by the time series plot in Figure 2e. Figure 2e presents the RKN LOS measurements along 80° MLAT as functions of magnetic longitude (MLON) and time. Similar to the snapshots, the color represents LOS speeds that project to the anti-sunward direction, and the flow of our interest appears as a region of red color. The time when THA and THD crossed the magnetopause was marked by the red arrows. The fact that the flow channel stayed quasi-steady during the satellite conjunction period suggests that the satellite measurements in Section 3.1.1 reflect the spatial distribution, rather than the temporal variation, of reconnection.

Figures 2a-c all observed a channel of fast anti-sunward flow in the pre-noon sector of the high latitude ionosphere, and the channel had a limited azimuthal extent. If the flow corresponded to a magnetopause reconnection, the X-line is expected to be located in the GSM-Y < 0 regime and spans over a limited local time range. This is consistent with the THEMIS satellite observation in Section 3.1.1, where THD at Y = -2.0 Re detected clear reconnection signatures, while THA at Y = 2.2 Re did not. In fact, if we project the satellite location to the ionosphere through field line tracing under the T89 model, THD was positioned close to the flow eastern boundary, while THA

Ann. Geophys. Discuss., https://doi.org/10.5194/angeo-2018-63
Manuscript under review for journal Ann. Geophys.
Discussion started: 3 July 2018

was far away (Figures 2a-c).

The radar observations thus provide critical information to interpret the in-situ reconnection extent. The X-line detected by THD did not extend duskward passing through the subsolar point of the magnetosphere; instead it extended dawnward towards the dawnside magnetopause. Note that the observations presented here do not rule out existence of other X-lines along the magnetopause, as there might exist other fast anti-sunward flows outside the radar FOVs. But those X-lines are not the focus of this study. It should also be noted that the determined flow extent is based on half of the maximum flow speed, which allows weak anti-sunward flows to extend beyond the flow boundaries. The weak flows are expected to correspond to weak background reconnection at the magnetopause. In fact, THA had detected weak reconnection signatures (i.e. weak plasma jets) 4-Re eastward of the active reconnection signatures at THD as found in Section 3.1.1, and this may agree with the weak ionospheric convection (green vectors in Figures 2a-c) eastward of the flow channel.

We quantitatively determine the flow extent in Figure 2f. Figure 2f shows the RKN LOS velocity profile along 80° MLAT at 1624 UT (the same time as Figures 2a-c) as a function of magnetic longitude and distance from 0° MLON. As mentioned above, the RKN LOS measurements captured the flow major component and thus approximated to the true 2-d velocities. Also shown is the SECS velocity profile. Here we only show the northward component of the SECS velocity as this component represents reconnecting flows across an azimuthally-aligned open-closed field line boundary. We quantify the flow azimuthal extent as the full-width-at-half-maximum (FWHM) of the velocity profile. But the LOS measurements only captured part of the flow channel, and could only reveal the half-width-at-half-maximum (HWHM) on one side of the velocity profile. The HWHM was 15° in MLON and 300 km at an altitude of 250 km. The SECS

Ann. Geophys. Discuss., https://doi.org/10.5194/angeo-2018-63
Manuscript under review for journal Ann. Geophys.
Discussion started: 3 July 2018

370 velocities covered the entire flow channel, and can be used to determine the FWHM. The FWHM
371 was 26° in MLON and 520 km.

372 To infer the X-line extent at the magnetopause, we project the flow width in the ionosphere to
373 the equatorial plane. This is done by mapping a pair of ionospheric locations that are azimuthally
374 separated around the THD footprint to the equatorial plane. The ratio of the pair separation in the
375 equatorial plane to that in the ionosphere gives a mapping factor. The mapping factor under T89
376 is 55, and this suggests the X-line local time extent to be ~4 Re.

377

378 3.2. Spatially patchy reconnection active at both satellites

379 3.2.1. In-situ satellite measurements

380 On April 19, 2015, under a southward IMF (Figure 3a), THA and THE crossed the
381 magnetopause nearly simultaneously (<2 min lag) with a 0.5 Re separation in Y (Figure 3b). They
382 passed from the magnetosheath into the magnetosphere. Both satellites observed jets in the V_L
383 component at the magnetopause. The jet at THA at ~1828:05 UT had a speed of 84% of and an
384 angle within ~15° from the Walen prediction. The jet at THE at ~1826:25 UT had a speed of 95%
385 of and an angle of ~29° from the Walen prediction. The ion distributions at THA and THE exhibit
386 clear D-shaped distributions, indicative of active reconnection at these two local times.

387

388 Section 3.2.2. Ground radar measurements

389 During the satellite measurements, the radars observed a channel of fast anti-sunward flow
390 around magnetic noon (Figures 4a-c). The flow crossed the open-closed field line boundary at 77°
391 MLAT, and qualifies for an ionospheric signature of magnetopause reconnection. The flow
392 direction was nearly parallel to the RKN radar beams, and therefore the RKN LOS measurements

Ann. Geophys. Discuss., https://doi.org/10.5194/angeo-2018-63
Manuscript under review for journal Ann. Geophys.
Discussion started: 3 July 2018

393 in Figure 4a approximated to the 2-d flow speed. The flow eastern boundary can be identified as
394 where the velocity dropped from red/orange to blue (dashed magenta line). Determining the flow
395 western boundary requires more measurements of the background convection velocity, which is
396 beyond the RKN FOV. But we again infer that the western boundary did not extend more than 1.5
397 h westward beyond the RKN FOV because the PGR and INV echoes there showed weakly
398 poleward and equatorward LOS speeds around the open-closed field line boundary. The CLY radar
399 data further indicated that the anti-sunward flow had started to rotate westward immediately
400 beyond the RKN FOV. This is because the CLY LOS velocities measured between the RKN and
401 INV radar FOVs were larger for more east-west oriented beams (appearing as yellow color) than
402 for more north-south oriented beams (green color). The rotation likely corresponds to the vortex
403 at the flow western boundary as sketched in *Oksavik et al.* [2004].
404 The more precise location of the western boundary can be retrieved from the SECS velocities
405 in Figure 4b and the SHF velocities in Figure 4c. The SECS velocities present a flow channel very
406 similar to that in Figure 4a, while the flow channel in the SHF velocities was more azimuthally-
407 aligned than in Figures 4a-b.
408 The determined flow extent agrees with the extent of the cusp in Figure 4d. The high spectral
409 widths associated with the cusp were located at the western half of the RKN FOV. They extended
410 westward beyond the RKN FOV into CLY far range gates, where they dropped from red to green
411 color. This is consistent with the inferred location and extent of the anti-sunward flow.
412 The flow of our interest just emerged from a weak background at the time when the THEMIS
413 satellites crossed the magnetopause (Figure 4e). This implies that the related reconnection just
414 initiated at the studied local time. The flow and the reconnection remained with a roughly steady
415 and localized extent after formation. We quantify the HWHM of the flow using the RKN LOS

velocity profile at 0830 UT (Figure 4f), and the HWHM was 10° MLON and 220 km. The FWHM is determined using the SECS velocities, and the FWHM was 26° MLON and 572 km. Such an FWHM corresponds to ~5 Re in the equatorial plane.

The fact that the fast anti-sunward flow had a limited azimuthal extent around magnetic noon implies that the corresponding magnetopause X-line should span over a limited local time range around the noon. This is consistent with the THEMIS satellite observation in Section 3.2.1, where reconnection was active at Y = 0.7 (THA) and 0.2 Re (THE). Projecting THA and THE locations to the ionosphere reveals that both satellite footprints were located within the flow longitudes. Therefore the reconnection at the two satellites was part of the same X-line around the subsolar point of the magnetopause. (The THE footprint was equatorward of THA because the X location of THE was closer to the Earth than THA. The magnetopause was expanding and it swept across THE and then THA.) The X-line further extended azimuthally beyond the two satellite locations, reaching a full length of ~5 Re.

3.3. Spatially continuous and extended reconnection active at both satellites

3.3.1. In-situ satellite measurements

On Apr 29, 2015, under a prolonged and steady southward IMF, THA and THE crossed the magnetopause successively with a time separation of ~30 min. The locations of the crossings were separated by 0.1-0.2 Re in the Y direction (Figure 5b). The satellites passed from the magnetosphere into the magnetosheath, and the magnetic field data suggest that the satellites crossed the current layer multiple times before completely entering the magnetosheath. We therefore only display the magnetic field and the plasma velocity in the GSM coordinates. Both satellites detected multiple flow jets, all agreeing with the Walen prediction with $\Delta V^* > 0.5$. For

Ann. Geophys. Discuss., https://doi.org/10.5194/angeo-2018-63
Manuscript under review for journal Ann. Geophys.
Discussion started: 3 July 2018

example, the jet at 1849-1850 UT measured by THA had a speed with 80% of and angle with 9° from the Walen prediction, and the jet at 1920-1922 UT by THE had a speed with 83% of and an angle with 1° from the Walen prediction. The ion distributions at THA and THE exhibit clear D-shaped distributions. Such observations suggest that reconnection was active at the THA and THE local times.

3.3.2. Ground radar measurements

In the ionosphere, the radars detected a fast anti-sunward flow as an ionospheric signature of the magnetopause reconnection (Figures 6a-c). The flow velocity here had a large component along the looking directions of the INV and CLY radars, and we therefore focus on the LOS measurements of these two radars. The flow had a broad azimuthal extent, as delineated by the dashed magenta lines (Figure 6a). A similar flow distribution is found in the SECS velocities (Figure 6b), and the SHF velocities (Figure 6c). Corresponding to the broad extent of the flow, the cusp had a broad extent (Figure 6d). The cusp continuously spanned across the INV and RKN FOVs and its western and eastern edges coincided with the western and eastern boundaries of the flow, supporting our delineation of the flow extent.

The wide flow channel in the ionosphere implies that the corresponding magnetopause X-line should be wide. Based on the flow distribution, we infer that much of the X-line should be located on the pre-noon sector, except that the eastern edge can extend across the magnetic noon meridian to the early post-noon sector. This inference is again consistent with the inference from the THA and THE measurements that the reconnection extended at least over the satellite separation (Y = -0.2 (THA) and 0 Re (THE)). Note, however, that the distance between THA and THE only covered <2% of the X-line extent determined from the ionosphere flow. While the satellite configuration

Ann. Geophys. Discuss., https://doi.org/10.5194/angeo-2018-63
Manuscript under review for journal Ann. Geophys.
Discussion started: 3 July 2018

and measurements here were similar to those in Section 3.2, the extent of reconnection was fundamentally different. This suggests that it is difficult to obtain a reliable estimate of the reconnection extent without the support of 2-d measurements and that satellites alone also cannot differentiate spatially extended reconnection from spatially patchy reconnection.

The flow temporal evolution is shown in Figures 6e-f, where the velocities are based on the LOS measurements from the CLY (Figure 6e) and INV (Figure 6f) radars. The velocities >-18° MLON are not useful and are shaded in grey. These measurements were from short range gates of the CLY radar, where the convection velocity is underestimated as the Doppler velocity is limited below the ion acoustic speed (~400 m/s) [*Haldoupis*, 1989; *Koustov et al*., 2005]. An overall wide flow channel is seen between ~-90° and -30° MLON for most of the studied time period, and in particular the flow azimuthal extent were nearly identical at the instances when THA and THE observed the reconnection. But between the two satellite observations, the flow experienced an interesting variation. The velocity at -74°−-30° MLON dropped by 100-200 m/s during 1900-1910 UT, while the velocity at -88°-74° MLON did not change substantially. The velocity enhanced again from 1910 UT. The enhancement first occurred at ~-60°−-40° MLON and then spread azimuthally towards east and west. The enhancement spread by 18° over 14 min at its eastern end (marked by the dashed magenta line), suggesting a spreading speed of 429 m/s. The spreading at the western end soon merged with the velocity enhancement at -88°-74° MLON, but a rough estimate suggests a speed of 444 km/s. It should be noted that the all three components of the IMF stayed steady for an extended time (Figure 7, discussed below in Section 3.4), and thus the evolution of the flow/reconnection was unlikely to be externally driven.

This sequence of changes gives an important implication that the extended X-line was a result of spreading of an initially patchy X-line. If we map the spreading in the ionosphere to the

485 magnetopause, the spreading occurred bi-directionally and at a speed of 24 km/s in each direction
486 based on field-line mapping under the T89 model (the mapping factor was 55). The spreading
487 process persisted for 10-20 min. Such an observation is similar to what has recently been reported
488 by *Zou et al.* [2018], where the X-lines also spread bi-directionally at a speed of a few tens of km/s.
489 However, the spreading in *Zou et al.* [2018] occurs following a southward turning of the IMF,
490 while the spreading here occurred without IMF variations. The mechanism of spreading is
491 explained either as motion of the current carriers of the reconnecting current sheet or as
492 propagation of the Alfven waves along the guide field [*Huba and Rudakov*, 2002; *Shay et al.* 2003;
493 *Lapenta et al.*, 2006; *Nakamura et al.*, 2012; *Jain et al.*, 2013].

494 It should be noted that X-line spreading can be a common process of reconnection that is not
495 limited to extended X-lines. A careful examination of Figure 4d suggests that spreading may have
496 also occurred for the patchy X-line (the eastern limit of the red/orange region spread from -36° to
497 -29° MLON during 1828-1832 UT). The two X-lines spread at a similarly speed, but duration of
498 the spreading process was two to three times longer in the extended than the patchy reconnection
499 events.

500 Figures 6g-h quantify the FWHM of the fast anti-sunward flow around the time when THA and
501 THE measured active reconnection. The width can be obtained based on the LOS measurements,
502 where we determine the HWHMs of the flow in the INV and CLY FOVs separately and add them
503 together as the FWHM. The FWHM was 63° MLON and 1260 km when THA measured the
504 reconnection, and was 62° MLON and 1240 km when THE measured the reconnection. This
505 corresponds to an X-line length of ~11 Re. Note that the determination of the HWHM inside the
506 CLY FOV has taken into account a background convection of ~400 m/s. The background came
507 from those plasmas moving azimuthally along the open-closed field line boundary but not crossing

Ann. Geophys. Discuss., https://doi.org/10.5194/angeo-2018-63
Manuscript under review for journal Ann. Geophys.
Discussion started: 3 July 2018

508 the boundary. The width can also be obtained based on the SECS measurements, which was 64°
509 MLON and 1280 km when THA measured the reconnection, and 60° MLON and 1200 km when
510 THE measured the reconnection. This is very close to the values derived from the LOS
511 measurements.
512
513 3.4. IMF and solar wind conditions for spatially patchy and extended reconnection
514 The above events definitely show that the local time extent of magnetopause reconnection X-
515 lines can vary from a few to >10 Re. Here we investigate whether and how the extent may depend
516 on the upstream driving conditions. Figure 7 presents the IMF, the solar wind velocity, and the
517 solar wind pressure taken from the OMNI data for the three events. The red vertical lines mark the
518 times when the reconnection was measured. The three events occurred under similar IMF field
519 strengths (5-6 nT), similar IMF Bz components (-3 nT), and similar solar wind velocities (300-400
520 km/s) and dynamic pressures (1-2 nPa), implying that the different X-line extents were unlikely
521 due to these parameters. This is different from *Milan et al.* [2016], who identified the solar wind
522 velocity as the controlling factor of reconnection extent. However, *Milan et al.* [2016] studied
523 reconnection under very strong IMF driving conditions when |B| ~15 nT, while our events occurred
524 under a more typical moderate driving (|B| ~5-6 nT).
525 The patchy X-line events had an IMF Bx of a larger magnitude than the extended reconnection
526 event did (4 vs. 0 nT). The patchy X-line events also had an IMF By component of a smaller
527 magnitude (2 vs. 5 nT), and with more variability on time scales of tens of minutes, than the
528 extended X-line event. The IMF Bx and By components are known to modify the magnetic shear
529 across the magnetopause and to affect the occurrence location of reconnection. The steady IMF
530 condition may allow X-lines to spread across local times unperturbedly, eventually reaching a wide

531 extent. Thus the X-line extent may depend on the IMF orientation and steadiness, although whether
532 and how they influence the extent needs to be further explored.
533
534 4. Summary
535 We carefully investigate the local time extent of magnetopause reconnection X-lines by
536 comparing the measurements of two THEMIS satellites and three ground radars. The radars
537 identify signatures of reconnection as fast ionospheric flows moving anti-sunward across the open-
538 closed field line boundary. When reconnection is active at only one of the two satellite locations,
539 only the ionosphere conjugate to this spacecraft shows a channel of fast anti-sunward flow. When
540 reconnection is active at both spacecraft and the spacecraft are separated by <1 Re, the ionosphere
541 conjugate to both spacecraft shows a channel of fast anti-sunward flow. The fact that the satellite
542 locations are mapped to the same flow channel suggests that the X-line is continuous between the
543 two satellites, and that it is appropriate to take the satellite separation as a lower limit estimate of
544 the X-line extent. Whether the X-line can still be regarded as continuous when the satellites are
545 separated by a few or > 10 Re is questionable, and needs to be examined using conjunctions with
546 a larger satellite separation than what have been presented here.
547 The X-line extent is measured as the extent of the ionospheric flow. In the three conjunction
548 events, the flows have an extent of 520, 572, and 1260 km in the ionosphere, which corresponds
549 to ~4, 5, and 11 Re at the magnetopause (under the T89 model) in the local time direction. This
550 provides strong observational evidence that magnetopause reconnection can occur over a wide
551 range of extents, from spatially patchy (a few Re) to spatially continuous and extended (>10 Re).
552 Interestingly, the extended reconnection is seen to initiate from a patchy reconnection, where the
553 X-line grows by spreading across local time. The speed of spreading is 50 km/s summing the

554 westward and eastward spreading motion, and the spreading process persists for 10-20 min.

555 The X-line extent may be affected by the IMF orientation and steadiness, although the
556 mechanism is not clearly known. For the modest solar wind driving conditions studied here, the
557 extended X-line occurs under a smaller IMF Bx component, and a larger and steadier IMF By
558 component than the patchy X-line. The IMF strength, the Bz component, and the solar wind
559 velocity and pressure are about the same for the extended and the patchy X-lines. Reconnection
560 can vary with time, even under steady IMF driving conditions.

561

562 **Acknowledgments.** This research was supported by the NASA Living With a Star Jack Eddy
563 Postdoctoral Fellowship Program, administered by UCAR's Cooperative Programs for the
564 Advancement of Earth System Science (CPAESS), NASA grant NNX15AI62G, NSF grants PLR-
565 1341359 and AGS-1451911, and AFOSR FA9550-15-1-0179 and FA9559-16-1-0364. The
566 THEMIS mission is supported by NASA contract NAS5-02099. SuperDARN is a collection of
567 radars funded by national scientific funding agencies. SuperDARN Canada is supported by the
568 Canada Foundation for Innovation, the Canadian Space Agency, and the Province of
569 Saskatchewan. We thank Tomoaki Hori for useful discussion on the SECS technique. Data
570 products of the SuperDARN, THEMIS, and OMNI are available at http://vt.superdarn.org/,
571 http://themis.ssl.berkeley.edu/index.shtml, and GSFC/SPDF OMNIWeb website.

572

573 Reference

574 Amm, O., A. Grocott, M. Lester, and T. K. Yeoman (2010), Local determination of ionospheric
575 plasma convection from coherent scatter radar data using the SECS technique, J. Geophys.
576 Res., 115, A03304, doi:10.1029/2009JA014832.

577 Alexeev, I. I., D. G. Sibeck, and S. Y. Bobrovnikov (1998), Concerning the location of
578 magnetopause merging as a function of the magnetopause current strength, J. Geophys.
579 Res., 103(A4), 6675–6684, doi:10.1029/97JA02863.
580 Angelopoulos, V. (2008), The THEMIS mission, Space Sci. Rev., 141, 5–34,
581 doi:10.1007/s11214-008-9336-1.
582 Auster, H. U., et al. (2008), The THEMIS fluxgate magnetometer, *Space Sci. Rev.*, **141**, 235–
583 264.
584 Baker, K. B., J. R. Dudeney, R. A. Greenwald, M. Pinnock, P. T. Newell, A. S. Rodger, N.
585 Mattin, and C.-I. Meng (1995), HF radar signatures of the cusp and low-latitude boundary
586 layer, J. Geophys. Res., 100(A5), 7671–7695, doi:10.1029/94JA01481.
587 Baker, K. B., A. S. Rodger, and G. Lu (1997), HF-radar observations of the dayside magnetic
588 merging rate: A Geospace Environment Modeling boundary layer campaign study, J.
589 Geophys. Res., 102(A5), 9603–9617, doi:10.1029/97JA00288.
590 Borovsky, J. E. (2013), Physical improvements to the solar wind reconnection control function for
591 the Earth's magnetosphere, J. Geophys. Res. Space Physics, 118, 2113–2121,
592 doi:10.1002/jgra.50110.
593 Bristow, W. A., D. L. Hampton, and A. Otto (2016), High-spatial-resolution velocity
594 measurements derived using Local Divergence-Free Fitting of SuperDARN observations, J.
595 Geophys. Res. Space Physics, 121, 1349–1361, doi:10.1002/2015JA021862.
596 Chisham, G., and Freeman, M. P. (2003): A technique for accurately determining the cusp-
597 region polar cap boundary using SuperDARN HF radar measurements, Ann. Geophys., 21,
598 983–996.
599 Cousins, E. D. P., and S. G. Shepherd (2010), A dynamical model of high-latitude convection
600 derived from SuperDARN plasma drift measurements, *J. Geophys. Res.*, 115, A12329,

doi:10.1029/2010JA016017.

Crooker, N. U. (1979), Dayside merging and cusp geometry, J. Geophys. Res., 84(A3), 951–959, doi:10.1029/JA084iA03p00951.

Crooker, N. U., F. R. Toffoletto, and M. S. Gussenhoven (1991), Opening the cusp, J. Geophys. Res., 96(A3), 3497–3503, doi: 10.1029/90JA02099.

Denig, W. F., W. J. Burke, N. C. Maynard, F. J. Rich, B. Jacobsen, P. E. Sandholt, A. Egeland, S. Leontjev, and V. G. Vorobjev (1993), Ionospheric signatures of dayside magnetopause transients: A case study using satellite and ground measurements, *J. Geophys. Res.*, **98**(A4), 5969–5980, doi:10.1029/92JA01541.

Dorelli, J. C., A. Bhattacharjee, and J. Raeder (2007), Separator reconnection at Earth's dayside magnetopause under generic northward interplanetary magnetic field conditions, J. Geophys. Res., 112, A02202, doi:10.1029/2006JA011877.

Dunlop, M. W., et al. (2011), Magnetopause reconnection across wide local time, *Ann. Geophys.*, **29**, 1683–1697, doi:10.5194/angeo-29-1683-2011.

Elphic, R. C., M. Lockwood, S. W. H. Cowley, and P. E. Sandholt (1990), Flux transfer events at the magnetopause and in the ionosphere, Geophys. Res. Lett., 17, 2241.

Fear, R. C., Milan, S. E., Fazakerley, A. N., Lucek, E. A., Cowley, S. W. H., and Dandouras, I.(2008), The azimuthal extent of three flux transfer events, Ann. Geophys., 26, 2353-2369, https://doi.org/10.5194/angeo-26-2353-2008.

Fear, R. C., S. E. Milan, E. A. Lucek, S. W. H. Cowley, and A. N. Fazakerley (2010), Mixed azimuthal scales of flux transfer events, in *The Cluster Active Archive – Studying the Earth's Space Plasma Environment*, Astrophys. Space Sci. Proc., edited by H. Laakso, M. Taylor, and C. P. Escoubet, pp. 389–398, Springer, Dordrecht, Netherlands, doi:10.1007/978-90-481-3499-1_27.

625 Glocer, A., J. Dorelli, G. Toth, C. M. Komar, and P. A. Cassak (2016), Separator reconnection at
626 the magnetopause for predominantly northward and southward IMF: Techniques and
627 results, J. Geophys. Res. Space Physics, 121, 140–156, doi:10.1002/2015JA021417.
628 Goertz, C. K., E. Nielsen, A. Korth, K. H. Glassmeier, C. Haldoupis, P. Hoeg, and D.
629 Hayward (1985), Observations of a possible ground signature of flux transfer events, J.
630 Geophys. Res., 90(A5), 4069–4078, doi:10.1029/JA090iA05p04069.
631 Gonzalez, W. D., and F. S. Mozer (1974), A quantitative model for the potential resulting from
632 reconnection with an arbitrary interplanetary magnetic field, J. Geophys. Res., 79(28), 4186–
633 4194, doi:10.1029/JA079i028p04186.
634 Greenwald, R. A., et al. (1995), DARN/SuperDARN: A global view of the dynamics of high-
635 latitude convection, Space Sci. Rev., 71, 761–796.
636 Haerendel, G., G. Paschmann, N. Sckopke, H. Rosenbauer, and P. C. Hedgecock (1978), The
637 frontside boundary layer of the magnetosphere and the problem of reconnection, J. Geophys.
638 Res., 83(A7), 3195–3216, doi:10.1029/JA083iA07p03195.
639 Haldoupis, C. (1989), A review on radio studies of auroral E-region ionospheric irregularities, *Ann.*
640 *Geophys.*, **7**, 239–258.
641 Hasegawa, H., et al. (2016), Decay of mesoscale flux transfer events during quasi‐continuous
642 spatially extended reconnection at the magnetopause, Geophys. Res. Lett., 43, 4755–4762,
643 doi:10.1002/2016GL069225.
644 Haynes, A. L., and C. E. Parnell (2010), A method for finding three-dimensional magnetic
645 skeletons, *Phys. Plasmas*, **17**, 092903, doi:10.1063/1.3467499.
646 Hesse, M., M. Kuznetsova, and J. Birn (2001), Particle-in-cell simulations of three-dimensional
647 collisionless magnetic reconnection, J. Geophys. Res., 106(A12), 29831–29841,

doi:10.1029/2001JA000075.

Huba, J. D., and L. I. Rudakov (2002), Three-dimensional Hall magnetic reconnection, Phys. Plasmas, 9, 4435.

Hudson, P. D. (1970), Discontinuities in an anisotropic plasma and their identification in the solar wind, Planet. Space Sci., 18, 1611–1622.

Jain, N., J. Büchner, S. Dorfman, H. Ji, and A. S. Sharma (2013), Current disruption and its spreading in collisionless magnetic reconnection, Phys. Plasmas 20, 112101.

Komar, C. M., P. A. Cassak, J. C. Dorelli, A. Glocer, and M. M. Kuznetsova (2013), Tracing magnetic separators and their dependence on IMF clock angle in global magnetospheric simulations, J. Geophys. Res. Space Physics, 118, 4998–5007, doi:10.1002/jgra.50479.

Komar, C. M., R. L. Fermo, and P. A. Cassak (2015), Comparative analysis of dayside magnetic reconnection models in global magnetosphere simulations, *J. Geophys. Res. Space Physics*, 120, 276–294, doi:10.1002/2014JA020587.

Koustov, A. V., D. W. Danskin, R. A. Makarevitch, and J. D. Gorin (2005), On the relationship between the velocity of E-region HF echoes and E B plasma drift, *Ann. Geophys.*, **23**(2), pp. 371–378, 0992-7689.

Laitinen, T. V., P. Janhunen, T. I. Pulkkinen, M. Palmroth, and H. E. J. Koskinen (2006), On the characterization of magnetic reconnection in global MHD simulations, *Ann. Geophys.*, **24**, 3059–3069.

Laitinen, T. V., M. Palmroth, T. I. Pulkkinen, P. Janhunen, and H. E. J. Koskinen (2007), Continuous reconnection line and pressure-dependent energy conversion on the magnetopause in a global MHD model, *J. Geophys. Res.*, **112**, A11201, doi:10.1029/2007JA012352.

671 Lapenta, G., D. Krauss-Varban, H. Karimabadi, J. D. Huba, L. I. Rudakov, and P.
672 Ricci (2006), Kinetic simulations of X-line expansion in 3D reconnection, Geophys. Res.
673 Lett., 33, L10102, doi:10.1029/2005GL025124.
674 Lee, L. C., and Z. F. Fu (1985), A theory of magnetic flux transfer at the earth's
675 magnetopause, *Geophys. Res. Lett.*, **12**, 105.
676 Lockwood, M., P. E. Sandholt, and S. W. H. Cowley, Dayside auroral activity and momentum
677 transfer from the solar wind, *Geophys. Res. Lett.*, **16**, 33, 1989.
678 Lockwood, M., M. F. Smith, Low altitude signatures of the cusp and flux transfer
679 events, *Geophys. Res. Lett.*, **16**, 879–882, 1989.
680 Lockwood, M., S. W. H. Cowley, P. E. Sandholt, and R. P. Lepping (1990), The ionospheric
681 signatures of flux transfer events and solar wind dynamic pressure changes, J. Geophys.
682 Res., 95(A10), 17113–17135, doi:10.1029/JA095iA10p17113.
683 Lockwood, M., and M. F. Smith (1994), Low and middle altitude cusp particle signatures for
684 general magnetopause reconnection rate variations: 1. Theory, *J. Geophys. Res.*, 99(A5),
685 8531–8553, doi:10.1029/93JA03399.
686 Lockwood, M., et al. (2001), Co-ordinated Cluster and ground-based instrument observations of
687 transient changes in the magnetopause boundary layer during an interval of predominantly
688 northward IMF: Relation to reconnection pulses and FTE signatures, *Ann.*
689 *Geophys.*, **19**, 1613–1640, doi:10.5194/angeo-19-1613-2001.
690 Luhmann, J. G., R. J. Walker, C. T. Russell, N. U. Crooker, J. R. Spreiter, and S. S.
691 Stahara (1984), Patterns of potential magnetic field merging sites on the dayside
692 magnetopause, *J. Geophys. Res.*, **89**, 1739–1742, doi:10.1029/JA089iA03p01739.
693 Lui, A. T. Y., and D. G. Sibeck, Dayside auroral activities and their implications for impulsive

694 entry processes in the dayside magnetosphere, *J. Atmos. Terr. Phys.*, **53**, 219, 1991.
695 McFadden, J. P., et al. (2008), The THEMIS ESA plasma instrument and in-flight
696 calibration, *Space Sci. Rev.*, **141**, 277–302.
697 McWilliams, K. A., T.K. Yeoman, and S.W.H. Cowley (2001a), Two-dimensional electric field
698 measurements in the ionospheric footprint of a flux transfer event, Annales Geophysicae,
699 18, pp. 1584–1598.
700 McWilliams, K. A., T.K. Yeoman, J.B. Sigwarth, L.A. Frank, and M. Brittnacher (2001b), The
701 dayside ultraviolet aurora and convection responses to a southward turning of the
702 interplanetary magnetic field, Annales Geophysicae, 17, pp. 707–721.
703 McWilliams, K. A., T.K. Yeoman, D.G. Sibeck, S.E. Milan, G.J. Sofko, T. Nagai, T. Mukai, I.J.
704 Coleman, T. Hori, and F.J. Rich (2004), Simultaneous observations of magnetopause flux
705 transfer events and of their associated signatures at ionospheric altitudes, Annales
706 Geophysicae, 22, pp. 2181–2199.
707 Milan, S. E., M. Lester, S. W. H. Cowley, and M. Brittnacher (2000), Convection and auroral
708 response to a southward turning of the IMF: Polar UVI, CUTLASS, and IMAGE signatures
709 of transient magnetic flux transfer at the magnetopause, J. Geophys. Res., 105(A7), 15741–
710 15755, doi:10.1029/2000JA900022.
711 Milan, S. E., S. M. Imber, J. A. Carter, M.-T. Walach, and B. Hubert (2016), What controls the
712 local time extent of flux transfer events?, J. Geophys. Res. Space Physics, 121, 1391–1401,
713 doi:10.1002/2015JA022012.
714 Moen, J., Carlson, H. C., Milan, S. E., Shumilov, N., Lybekk, B., Sandholt, P. E., and Lester, M.:
715 On the collocation between dayside auroral activity and coherent HF radar backscatter,
716 Ann. Geophys., 18, 1531-1549, https://doi.org/10.1007/s00585-001-1531-2, 2000.

717 Moore, T. E., M.-C. Fok, and M. O. Chandler, The dayside reconnection X line, J. Geophys.
718 Res., 107(A10), 1332, doi:10.1029/2002JA009381, 2002.
719 Nakamura, T. K. M., R. Nakamura, A. Alexandrova, Y. Kubota, and T. Nagai (2012), Hall
720 magnetohydrodynamic effects for three-dimensional magnetic reconnection with finite
721 width along the direction of the current, J. Geophys. Res., 117, A03220,
722 doi:10.1029/2011JA017006.
723 Neudegg, D. A., T. K. Yeoman, S. W. H. Cowley, G. Provan, G. Haerendel, W. Baumjohann, U.
724 Auster, K.-H. Fornacon, E. Georgescu, and C. J. Owen (1999), A¯flux transfer event
725 observed at the magnetopause by the Equator-S spacecraft and in the ionosphere by the
726 CUTLASS HF radar, Ann. Geophysicae, 17, 707.
727 Neudegg, D. A., et al. (2000), A survey of magnetopause FTEs and associated flow bursts in the
728 polar ionosphere, *Ann. Geophys.*, **18**, 416.
729 Nishitani, N., T. Ogawa, M. Pinnock, M. P. Freeman, J. R. Dudeney, J.-P. Villain, K. B.
730 Baker, N. Sato, H. Yamagishi, and H. Matsumoto (1999), A very large scale flow burst
731 observed by the SuperDARN radars, J. Geophys. Res., 104(A10), 22469–22486,
732 doi:10.1029/1999JA900241.
733 Newell, P. T., C.-I. Meng, D. G. Sibeck, and R. Lepping (1989), Some low-altitude cusp
734 dependencies on the interplanetary magnetic field, J. Geophys. Res., 94(A7), 8921–8927,
735 doi:10.1029/JA094iA07p08921.
736 Newell, P. T., and C. ‐ I. Meng (1994), Ionospheric projections of magnetospheric regions under
737 low and high solar wind conditions, J. Geophys. Res., 99, 273.
738 Newell, P. T., S. Wing, and F. J. Rich (2007), Cusp for high and low merging rates, *J. Geophys.*
739 *Res.*, 112, A09205, doi:10.1029/2007JA012353.

740 Newell, P. T., T. Sotirelis, K. Liou, C. - I. Meng, and F. J. Rich (2007b), A nearly universal solar
741 wind - magnetosphere coupling function inferred from 10 magnetospheric state variables, J.
742 Geophys. Res., 112, A01206, doi: 10.1029/2006JA012015.
743 Tsyganenko, N. A. (1995), Modeling the Earth's magnetospheric magnetic field confined within
744 a realistic magnetopause, J. Geophys. Res., 100(A4), 5599–5612, doi:10.1029/94JA03193.
745 Oksavik, K., J. Moen, and H. C. Carlson (2004), High-resolution observations of the small-scale
746 flow pattern associated with a poleward moving auroral form in the cusp, *Geophys. Res.*
747 *Lett.*, **31**, L11807, doi:10.1029/2004GL019838.
748 Oksavik, K., J. Moen, H. C. Carlson, R. A. Greenwald, S. E. Milan, M. Lester, W. F. Denig,
749 and R. J. Barnes (2005), Multi-instrument mapping of the small-scale flow dynamics related
750 to a cusp auroral transient, *Ann. Geophys.*, **23**, 2657–2670.
751 Paschmann, G., et al. (1979), Plasma acceleration at the Earth's magnetopause: Evidence for
752 magnetic reconnection, Nature, 282, 243.
753 Paschmann, G., et al. (1986), The magnetopause for large magnetic shear: AMPTE/IRM
754 observations, *J. Geophys. Res.*, **91**, 11,099.
755 Phan, T.-D., et al. (2000), Extended magnetic reconnection at the Earth's magnetopause from
756 detection of bi-directional jets, *Nature*, **404**, 848.
757 Phan, T. D., H. Hasegawa, M. Fujimoto, M. Oieroset, T. Mukai, R. P. Lin, and W. R.
758 Paterson (2006), Simultaneous Geotail and Wind observations of reconnection at the
759 subsolar and tail flank magnetopause, Geophys. Res. Lett., 33, L09104,
760 doi:10.1029/2006GL025756.
761 Phan, T. D., G. Paschmann, J. T. Gosling, M. Oieroset, M. Fujimoto, J. F. Drake, and V.
762 Angelopoulos (2013), The dependence of magnetic reconnection on plasma β and magnetic

shear: Evidence from magnetopause observations, Geophys. Res. Lett., 40, 11–16, doi:10.1029/2012GL054528.

Pinnock, M & Rodger, A. (2001). On determining the noon polar cap boundary from SuperDARN HF radar backscatter characteristics. Annales Geophysicae. 18. 10.1007/s00585-001-1523-2.

Pinnock, M., Rodger, A. S., Dudeney, J. R., Baker, K. B., Newell, P. T., Greenwald, R. A., and Greenspan, M. E. (1993): Observations of an enhanced convection channel in the cusp ionosphere, J. Geophys. Res., 98, 3767–3776.

Pinnock, M., A. S. Rodger, J. R. Dudeney, F. Rich, and K. B. Baker (1995), High spatial and temporal resolution observations of the ionospheric cusps, *Ann. Geophys.*, **13**, 919–925.

Provan, G. & Yeoman, T.K. (1999), Statistical observations of the MLT, latitude and size of pulsed ionospheric flows with the CUTLASS Finland radar, Annales Geophysicae, 17: 855. https://doi.org/10.1007/s00585-999-0855-1

Provan, G., T. K. Yeoman, and S. E. Milan (1998), CUTLASS Finland radar observations of the ionospheric signatures of flux transfer events and the resulting plasma flows, *Ann. Geophys.*, **16**, 1411–1422.

Ruohoniemi, J. M., R. A. Greenwald, K. B. Baker, J.-P. Villain, C. Hanuise, and J. Kelly (1989), Mapping high-latitude plasma convection with coherent HF radars, J. Geophys. Res., 94(A10), 13463–13477, doi:10.1029/JA094iA10p13463.

Ruohoniemi, J. M., and K. B. Baker (1998), Large-scale imaging of high-latitude convection with Super Dual Auroral Radar Network HF radar observations, J. Geophys. Res., 103(A9), 20797–20811, doi:10.1029/98JA01288.

Russell, C. T., and R. C. Elphic (1979), ISEE observations of flux transfer events at the dayside

magnetopause, Geophys. Res. Lett., 6(1), 33–36, doi:10.1029/GL006i001p00033.

Sandholt, P. E., C. S. Deehr, A. Egeland, B. Lybekk, R. Viereck, and G. J. Romick (1986), Signatures in the dayside aurora of plasma transfer from the magnetosheath, J. Geophys. Res., 91(A9), 10063–10079, doi:10.1029/JA091iA09p10063.

Sandholt, P. E., M. Lockwood, T. Oguti, S. W. H. Cowley, K. S. C. Freeman, B. Lybekk, A. Egeland, and D. M. Willis (1990), Midday auroral breakup events and related energy and momentum transfer from the magnetosheath, J. Geophys. Res., 95(A2), 1039–1060, doi:10.1029/JA095iA02p01039.

Sandholt, P. E., et al. (1994), Cusp/cleft auroral activity in relation to solar wind dynamic pressure, interplanetary magnetic field B_z and B_y , J. Geophys. Res., 99(A9), 17323–17342, doi:10.1029/94JA00679.

Scholer, M. (1988), Magnetic flux transfer at the magnetopause based on single x line bursty reconnection, *Geophys. Res. Lett.*, **15**, 291.

Scholer, M., I. Sidorenko, C. H. Jaroschek, R. A. Treumann, and A. Zeiler (2003), Onset of collisionless magnetic reconnection in thin current sheets: Three-dimensional particle simulations, *Phys. Plasmas*, **10**(9), 3521–3527.

Shay, M. A., J. F. Drake, M. Swisdak, W. Dorland, and B. N. Rogers (2003), Inherently three dimensional magnetic reconnection: A mechanism for bursty bulk flows? Geophys. Res. Lett., 30(6), 1345, doi:10.1029/2002GL016267.

Shepherd, L. S., and P. A. Cassak (2012), Guide field dependence of 3-D X-line spreading during collisionless magnetic reconnection, J. Geophys. Res., 117, A10101, doi:10.1029/2012JA017867.

Smith, M. F.M. Lockwood, S.W.H. Cowley, The statistical cusp: a simple flux transfer event

model, *Planet Space Sci.*, 1992

Sonnerup, B. U. Ö., and L. J. Cahill Jr. (1967), Magnetopause structure and attitude from Explorer 12 observations, *J. Geophys. Res.*, **72**, 171.

Sonnerup, B. U. (1974), Magnetopause reconnection rate, J. Geophys. Res., 79(10), 1546–1549, doi:10.1029/JA079i010p01546.

Southwood, D. J. (1985), Theoretical aspects of ionosphere - magnetosphere - solar wind coupling, Adv. Space Res., 5(4), 7–14, doi:10.1016/0273 - 1177(85)90110 - 3.

Southwood, D. J. (1987), The ionospheric signature of flux transfer events, *J. Geophys. Res.*, **92**, 3207.

Swisdak, M., and J. F. Drake (2007), Orientation of the reconnection X-line, Geophys. Res. Lett., 34, L11106, doi:10.1029/2007GL029815.

Southwood, D. J., C. J. Farrugia, and M. A. Saunders (1988), What are flux transfer events? *Planet. Space Sci.*, **36**, 503.

Thorolfsson, A., J.-C. Cerisier, M. Lockwood, P. E. Sandholt, C. Senior, and M. Lester (2000), Simultaneous optical and radar signatures of poleward-moving auroral forms, *Ann. Geophys.*, **18**, 1054.

Trattner, K. J., J. S. Mulcock, S. M. Petrinec, and S. A. Fuselier (2007), Probing the boundary between antiparallel and component reconnection during southward interplanetary magnetic field conditions, *J. Geophys. Res.*, 112, A08210, doi:10.1029/2007JA012270.

Tsyganenko, N. A., A magnetospheric magnetic field model with a warped tail current sheet, Planet. Space Sci., 87, 5, 1989

Tsyganenko, N. A. (1995), Modeling the Earth's magnetospheric magnetic field confined within a realistic magnetopause, J. Geophys. Res., 100(A4), 5599–5612,

doi:10.1029/94JA03193.

Tsyganenko, N. A. (2002a), A model of the magnetosphere with a dawn-dusk asymmetry, 1, Mathematical structure, J. Geophys. Res., 107(A8), doi:10.1029/2001JA000219.

Tsyganenko, N. A. (2002b), A model of the near magnetosphere with a dawn-dusk asymmetry, 2, Parameterization and fitting to observations, J. Geophys. Res., 107(A8), doi:10.1029/2001JA000220.

Walsh, B. M., J. C. Foster, P. J. Erickson, and D. G. Sibeck (2014a), Simultaneous ground- and space-based observations of the plasmaspheric plume and reconnection, *Science*, **343**, 1122–1125, doi:10.1126/science.1247212.

Walsh, B. M., T. D. Phan, D. G. Sibeck, and V. M. Souza (2014b), The plasmaspheric plume and magnetopause reconnection, Geophys. Res. Lett., 41, 223–228, doi:10.1002/2013GL058802.

Walsh, B. M., C. M. Komar, and Y. Pfau-Kempf (2017), Spacecraft measurements constraining the spatial extent of a magnetopause reconnection X line, Geophys. Res. Lett., 44, 3038–3046, doi:10.1002/2017GL073379.

Wang, Y., et al. (2005), Initial results of high-latitude magnetopause and low-latitude flank flux transfer events from 3 years of Cluster observations, J. Geophys. Res., 110, A11221, doi:10.1029/2005JA011150.

Wang, J., et al. (2007), TC1 and Cluster observation of an FTE on 4 January 2005: A close conjunction, Geophys. Res. Lett., 34, L03106, doi:10.1029/2006GL028241.

Wild, J. A., Cowley, S. W. H., Davies, J. A., Khan, H., Lester, M., Milan, S. E., Provan, G., Yeoman, T. K., Balogh, A., Dunlop, M. W., Fornacon, K.-H., and Georgescu, E. (2001): First simultaneous observations of flux transfer events at the high-latitude magnetopause by the Cluster spacecraft and pulsed radar signatures in the conjugate ionosphere by the CUTLASS

and EISCAT radars, Ann. Geophys., 19, 1491–1508.

Wild, J. A., Milan, S. E., Davies, J. A., Cowley, S. W. H., Carr, C. M., and Balogh, A.(2005): Double Star, Cluster, and groundbased observations of magnetic reconnection during an interval of duskward oriented IMF: preliminary results, Ann. Geophys., 23, 2903–2907

Wild, J. A., Milan, S. E., Davies, J. A., Dunlop, M. W., Wright, D. M., Carr, C. M., Balogh, A., Reme, H., Fazakerley, A. N., ` and Marchaudon, A. (2007): On the location of dayside magnetic reconnection during an interval of duskward oriented IMF, Ann. Geophys., 25, 219–238.

Zhang, Q.-H., et al. (2008), Simultaneous tracking of reconnected flux tubes: Cluster and conjugate SuperDARN observations on 1 April 2004, *Ann. Geophys.*, **26**, 1545–1557, doi:10.5194/angeo-26-1545-2008.

Zou, Y., Walsh, B. M., Nishimura, Y., Angelopoulos, V., Ruohoniemi, J. M., McWilliams, K. A., & Nishitani, N. (2018). Spreading speed of magnetopause reconnection X-lines using ground-satellite coordination. Geophysical Research Letters, 45. https://doi.org/10.1002/2017GL075765

878 Figure 1. Measurements from THD and THA during their nearly simultaneous crossings of the
879 magnetopause on March 11, 2014. Figure 1a: OMNI IMF condition. Figure 1b: THD and THA
880 locations projected to the GSM X-Y plane. The dashed curve marks the magnetopause and the
881 dotted curve marks the bow shock. Figures 1c-f: THD measured magnetic field (0.25 s resolution),
882 ion energy flux (3 s), ion density (3 s), and ion velocity (3 s). The ion measurements were taken
883 from ground ESA moments. The magnetic field and the ion velocity components are displayed in
884 the LMN boundary normal coordinate system. The magnetopause crossing is shaded in pink.
885 Figure 1g: THD ion distribution function on the bulk velocity-magnetic field plane. The small
886 black line indicates the direction and the bulk velocity of the distributions. Figures 1h-l: THA
887 measurements in the same format as in Figures 1c-g.
888
889 Figure 2. Ionospheric velocity field at the cusp when the THEMIS satellites crossed the
890 magnetopause on March 11, 2014. Figure 2a: SuperDARN LOS speeds (color tiles) and merged
891 velocity vectors (color arrows) in the Altitude adjusted corrected geomagnetic (AACGM)
892 coordinates. The FOVs of the RKN, INV, and CLY radars are outlined with the black dashed lines.
893 The colors of the tiles indicate the LOS speeds away from the radar. The colors and the lengths of
894 the arrows indicate the merged velocity magnitudes and the arrow directions indicate the velocity
895 directions. Red and anti-sunward directed flows are the ionospheric signature of magnetopause
896 reconnection. The dashed magenta lines mark the flow western and eastern boundaries. The
897 satellite footprints under the T89 are shown as the THD and THA marker. Figure 2b: Similar to
898 Figure 2a but showing SECS velocity vectors (color arrows). Figure 2c: Similar to Figure 2a but
899 showing SHF velocity vectors (color arrows). Figure 2d: SuperDARN spectral width
900 measurements (color tiles). The red contour marks the cusp. Figure 2e: Time evolution of RKN

LOS velocities along 80° MLAT. The velocities are color coded in the same way as Figure 2a. Figure 2f: Longitudinal profile of convection velocities along 80° MLAT at 1622 UT. The profiles is also shown as a function of the distance measured azimuthally from 0° MLON. The profile in black is based on the RKN LOS measurements, from which the HWHM is determined and marked by the black arrow. The profile in red is based on the northward components of the SECS velocities, from which the FWHM is determined and marked by the red arrow. The dotted black and red vertical lines are the drop lines of the HWHM and FWHM, respectively.

Figure 3. Measurements from THA and THE during their nearly simultaneous crossings of the magnetopause on Apr 19, 2015. The figure format is similar to Figure 1.

Figure 4. Ionospheric velocity field at the cusp when the THEMIS satellites crossed the magnetopause on Apr 19, 2015. The figure format is similar to Figure 2. The velocity time evolution in Figure 4e and the velocity profile in Figure 4f are taken along 79 °MLAT.

Figure 5. Measurements from THA and THE during their crossings of the magnetopause on Apr 29, 2015. The figure format is similar to Figure 1, but the magnetic field and plasma velocities are displayed in the GSM coordinates.

Figure 6. Figures 6a-d: Ionospheric velocity field at the cusp when the THEMIS satellites crossed the magnetopause on Apr 29, 2015. The figure format is similar to Figures 2a-d except that in Figure 6a the color of the CLY color tiles represent LOS speeds towards the radar as here LOS speeds towards the CLY radar project to the anti-sunward direction. Figures 6e-f: Time evolution

Ann. Geophys. Discuss., https://doi.org/10.5194/angeo-2018-63
Manuscript under review for journal Ann. Geophys.
Discussion started: 3 July 2018

924 of LOS velocities along 80° MLAT from the INV and CLY radars. The velocity measurements in
925 the shaded region are backscatters from the E-region ionosphere and thus underestimate the
926 convection speed. The flow channel spread azimuthally before reaching an extended extent, and
927 the time-dependent locations of its western and eastern boundaries are marked by the dashed
928 magenta lines. Figures 6g-h: Longitudinal profiles of the LOS and the poleward SECS velocities
929 along 80° MLAT when THA and THE observed reconnection.
930
931 Figure 7. Comparison of the IMF and solar wind driving conditions between the reconnection
932 events on March 11, 2014, Apr 19, 2015, and Apr 29, 2015. From top to bottom: IMF in GSM
933 coordinates, solar wind speed, and solar wind dynamic pressure. The red vertical lines mark the
934 times of the satellite-ground conjunction.
935
936
937

Ann. Geophys. Discuss., https://doi.org/10.5194/angeo-2018-63
Manuscript under review for journal Ann. Geophys.
Discussion started: 3 July 2018

938 Figure 1.

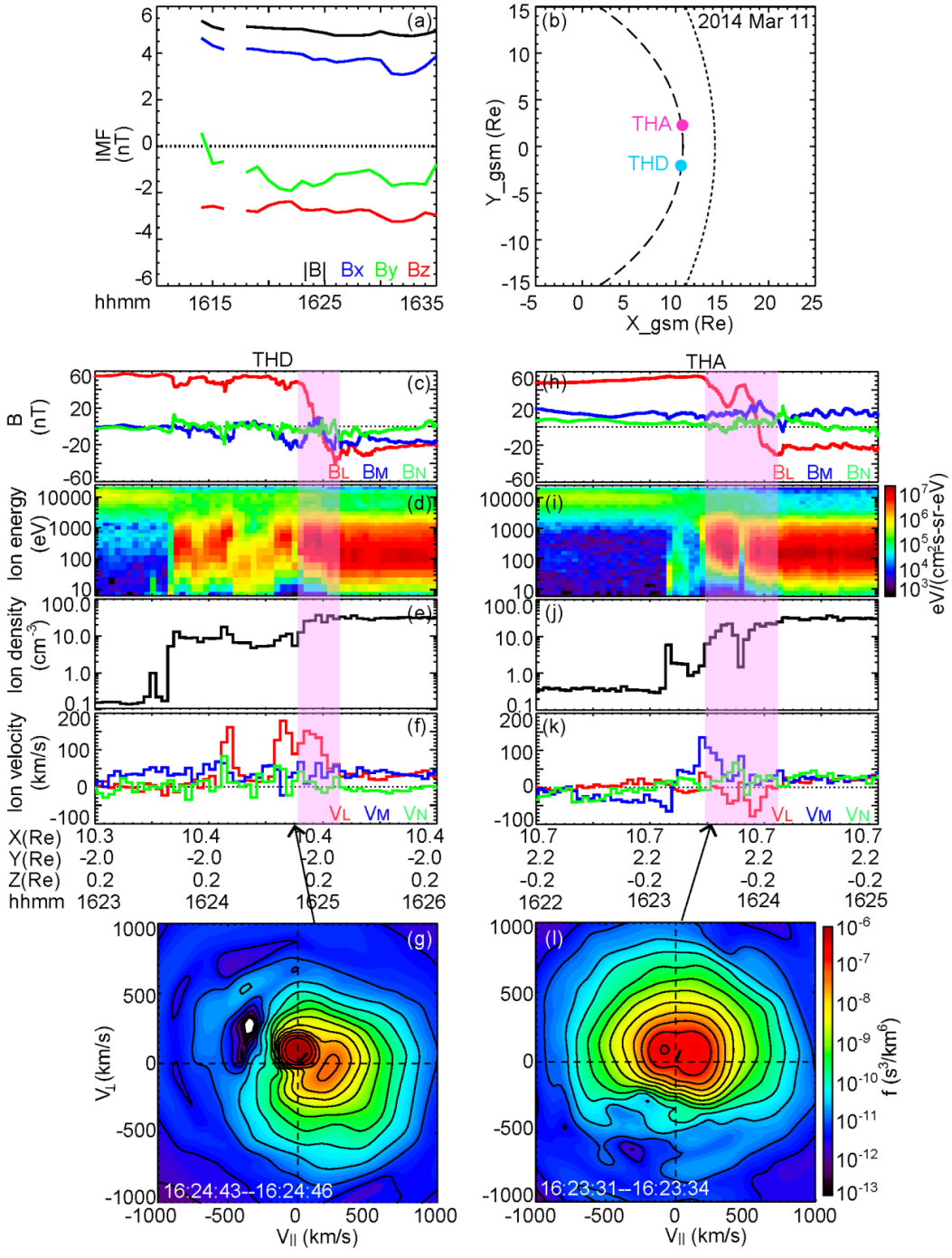

939

Ann. Geophys. Discuss., https://doi.org/10.5194/angeo-2018-63
Manuscript under review for journal Ann. Geophys.
Discussion started: 3 July 2018

940 Figure 2.

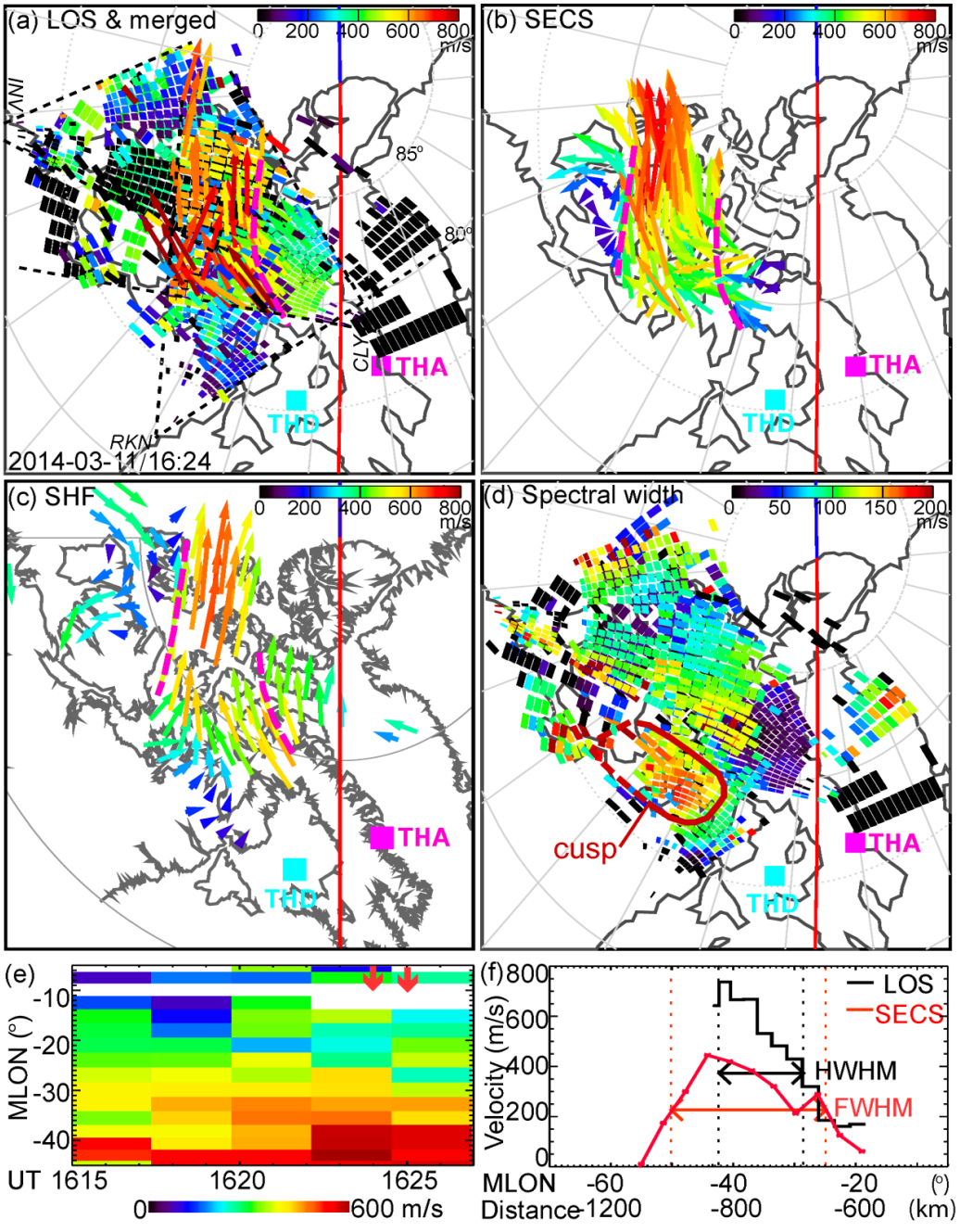

941

942

Ann. Geophys. Discuss., https://doi.org/10.5194/angeo-2018-63
Manuscript under review for journal Ann. Geophys.
Discussion started: 3 July 2018

943 Figure 3,

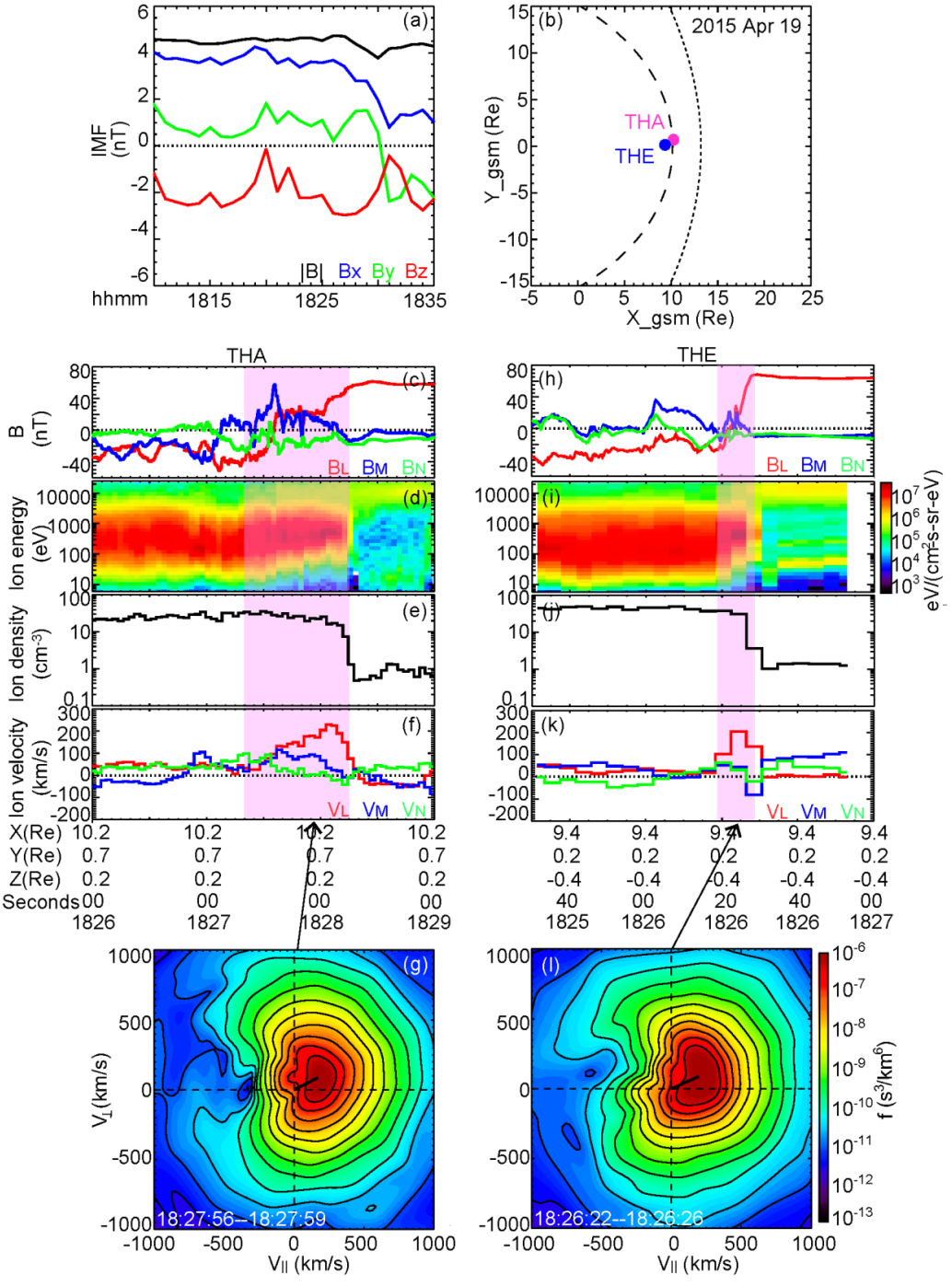

944

Ann. Geophys. Discuss., https://doi.org/10.5194/angeo-2018-63
Manuscript under review for journal Ann. Geophys.
Discussion started: 3 July 2018

Annales Geophysicae Discussions
Open Access
EGU

945 Figure 4,

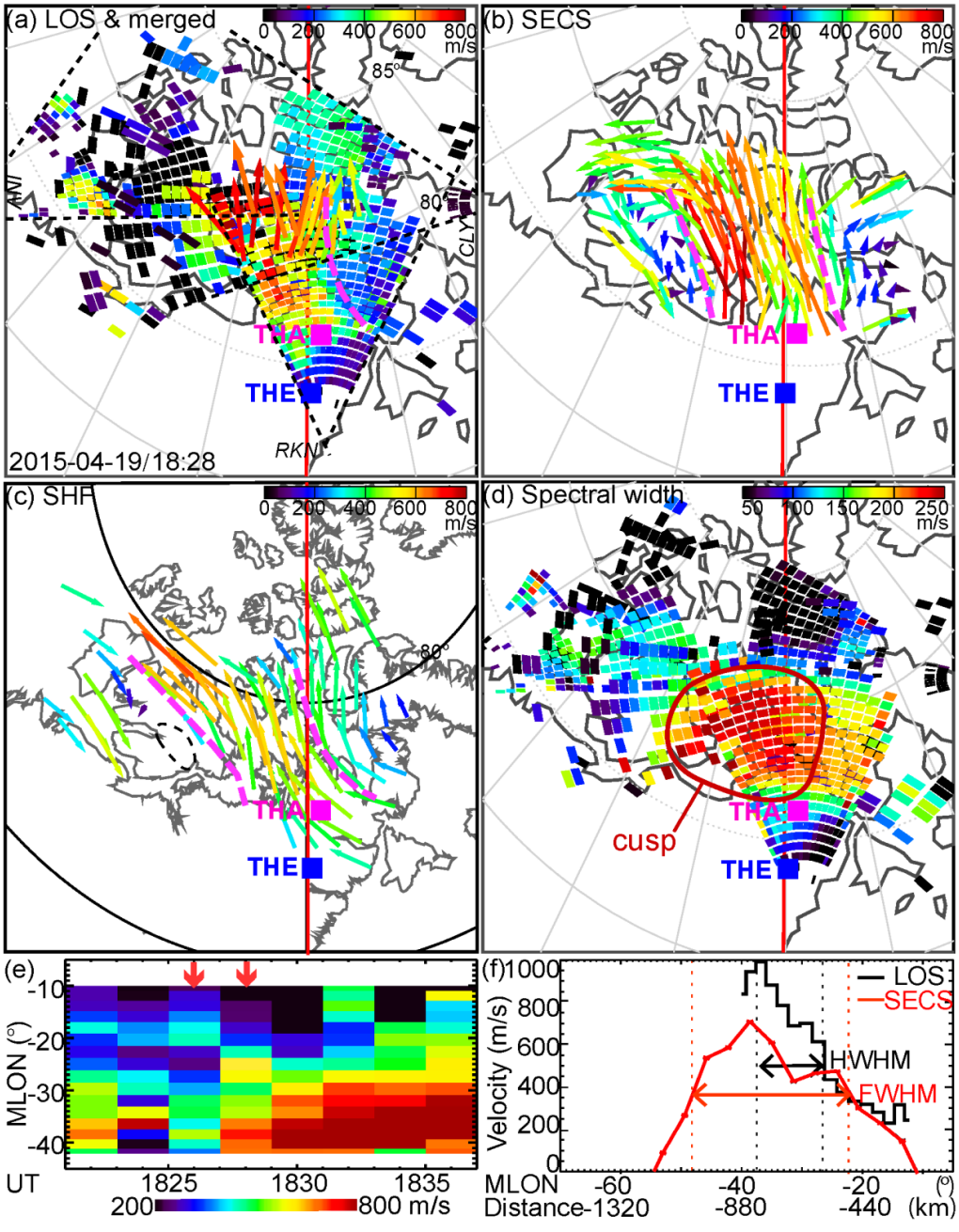

946

Ann. Geophys. Discuss., https://doi.org/10.5194/angeo-2018-63
Manuscript under review for journal Ann. Geophys.
Discussion started: 3 July 2018

Annales Geophysicae Discussions
Open Access
EGU

947 Figure 5.

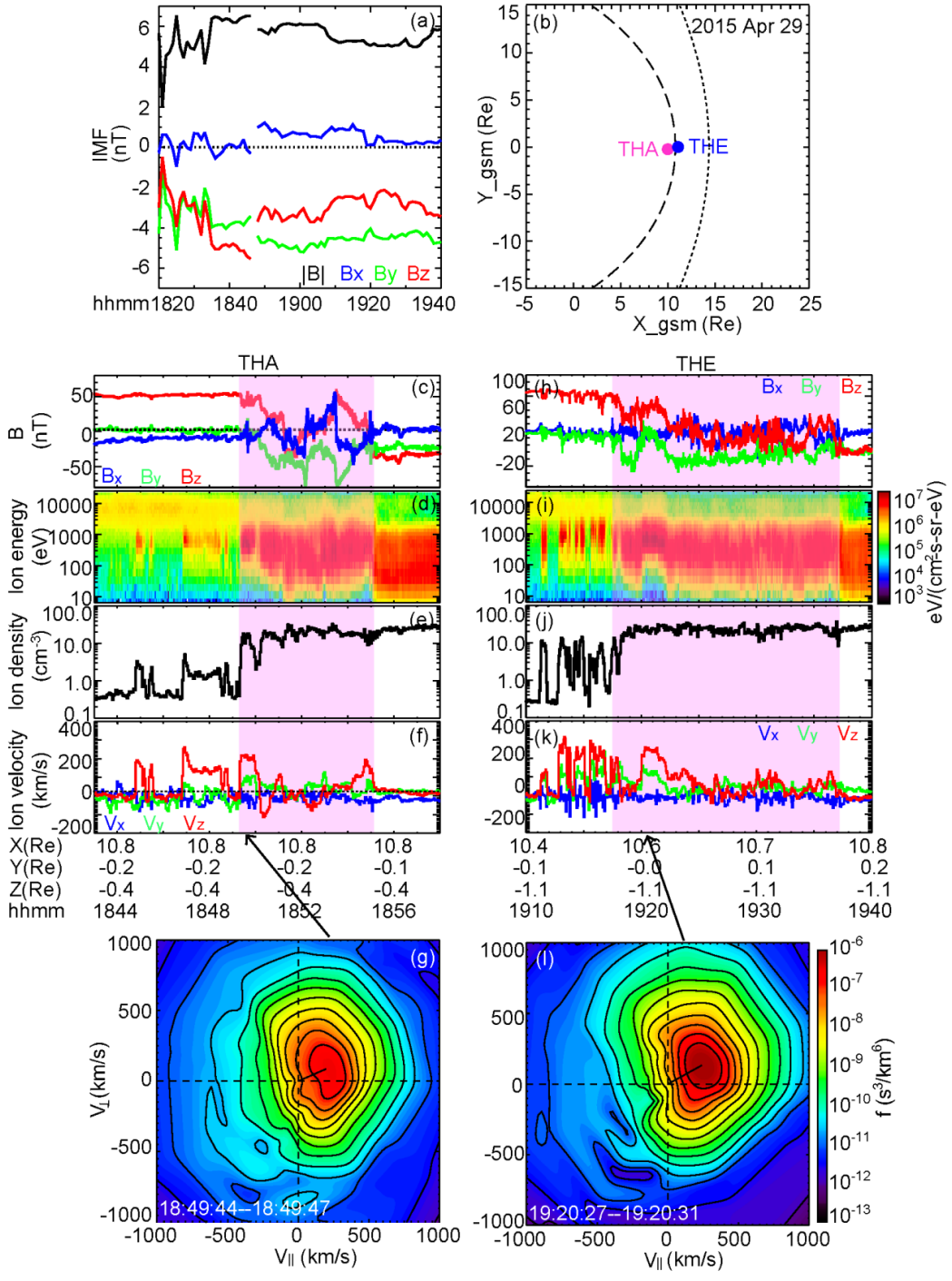

948

Ann. Geophys. Discuss., https://doi.org/10.5194/angeo-2018-63
Manuscript under review for journal Ann. Geophys.
Discussion started: 3 July 2018

949 Figure 6.

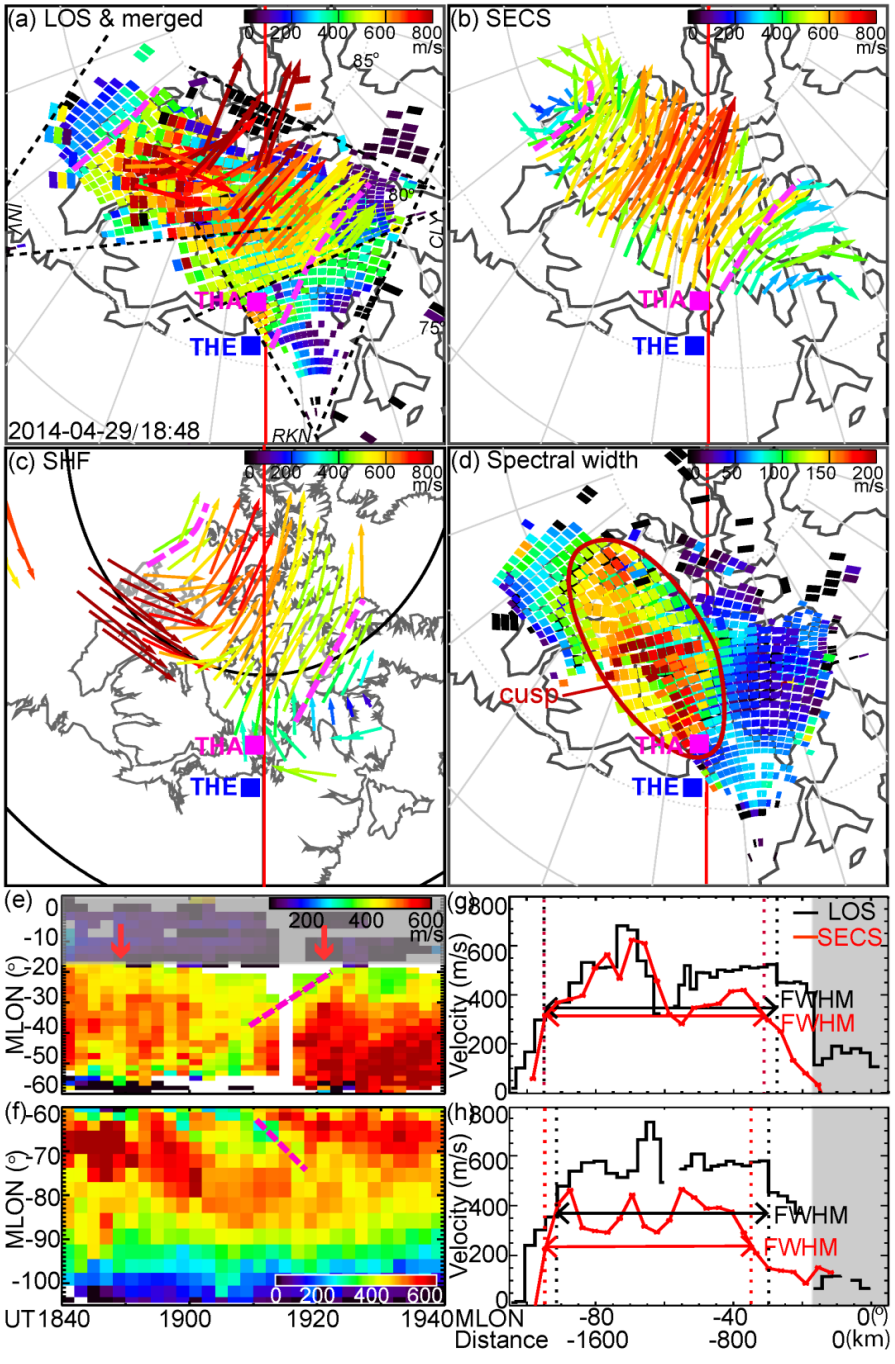

950

Ann. Geophys. Discuss., https://doi.org/10.5194/angeo-2018-63
Manuscript under review for journal Ann. Geophys.
Discussion started: 3 July 2018

Annales Geophysicae Discussions
Open Access
EGU

951 Figure 7.

952

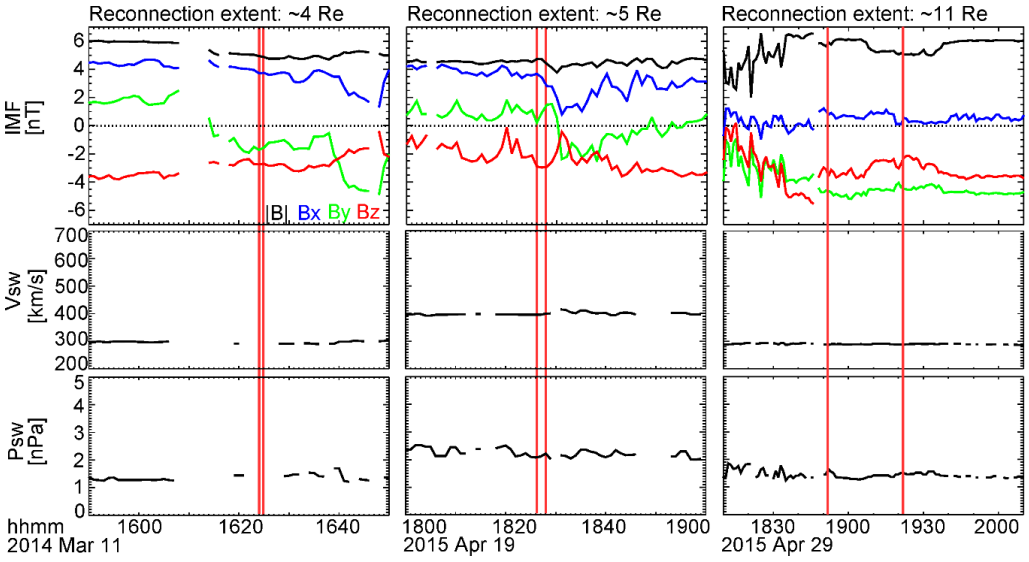

953

954

955

956

957

958

959

960

961

962

963

964

965